CrossMark

RESEARCH PAPER

A two-parameter model to predict fatigue life of high-strength steels in a very high cycle fatigue regime

Chengqi Sun[1] · Xiaolong Liu[1] · Youshi Hong[1]

Abstract   In this paper, ultrasonic (20 kHz) fatigue tests were performed on specimens of a high-strength steel in very high cycle fatigue (VHCF) regime. Experimental results showed that for most tested specimens failed in a VHCF regime, a fatigue crack originated from the interior of specimen with a fish-eye pattern, which contained a fine granular area (FGA) centered by an inclusion as the crack origin. Then, a two-parameter model is proposed to predict the fatigue life of high-strength steels with fish-eye mode failure in a VHCF regime, which takes into account the inclusion size and the FGA size. The model was verified by the data of present experiments and those in the literature. Furthermore, an analytic formula was obtained for estimating the equivalent crack growth rate within the FGA. The results also indicated that the stress intensity factor range at the front of the FGA varies within a small range, which is irrespective of stress amplitude and fatigue life.

Keywords   Very high-cycle fatigue · High-strength steels · Fatigue life · Inclusion size · Crack growth rate

1 Introduction

Very high cycle fatigue (VHCF) behavior of metallic materials has become an important research topic [1–11] due to the fact that modern industries often require metallic components to endure exceeding 10^8 loading cycles of safe performance

in service. For example, train axles rotate about 10^9 cycles when a high speed train runs at 2.4×10^6 km. Different from low cycle fatigue, the crack initiation site of VHCF usually locates in the interior of a specimen instead of initiating from the surface due to a persistent slip. For high-strength steels, the failure of VHCF is mostly caused by interior nonmetallic inclusions and a fish-eye pattern often presented with an embedded morphology of a fine granular area (FGA) [12] around the inclusion of the crack origin, which is also named the optical dark area [13] or granular-bright-facet [14]. The study by Murakami et al. [15] showed that the FGA played a crucial role in VHCF failure and that the relative size of the FGA to that of the inclusion at the crack origin increased with the increase of the fatigue life. Zhao et al. [16] investigated the formation of the mechanism of FGA in high-strength steels and presented a theoretical model to predict the threshold value of its formation based on the plastic zone size at the crack tip. It was shown that the stress intensity factor range at the front of the FGA was a constant and was close to the threshold value of the crack propagation ΔK_{th}. In crack initiation and early growth stage of VHCF, the crack growth rate is much lower than 10^{-10} m/cycle [13,17–20], and more than 90 % of fatigue life is consumed to form the FGA [21–25]. Therefore, it is essential to develop a model to predict the fatigue life in relation to FGA. Some methods have been proposed to predict the fatigue life or fatigue strength of high-strength steels in the VHCF regime by incorporating the effect of inclusion size at the crack origin [21,26–28]. For example, Wang et al. [29] incorporated fatigue life into Murakami's model [30] and proposed

✉ Youshi Hong
  hongys@imech.ac.cn

[1] The State Key Laboratory of Nonlinear Mechanics, Institute of Mechanics, Chinese Academy of Sciences, Beijing 100190, China

$$\sigma_a = \frac{\beta(Hv + 120)}{(\sqrt{area})^{1/6}} \left(\frac{1-R}{2} \right)^\alpha, \tag{1}$$
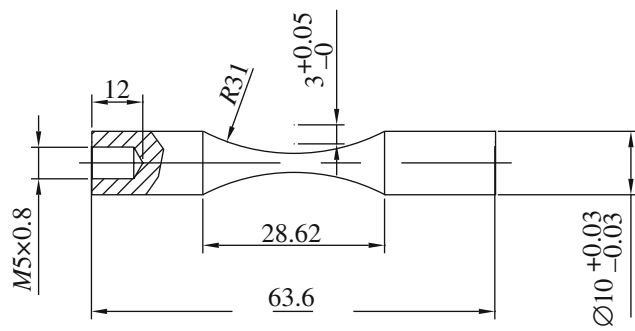
Fig. 1 Geometry of hourglass shape specimen for fatigue testing, dimensions in mm

where $\beta = 3.09 - 0.12 \log N_f$ for interior inclusions or defects and $\beta = 2.79 - 0.108 \log N_f$ for surface inclusions or defects for four low-alloy high-strength steels.

Akiniwa et al. [31] assumed the Paris relation was still valid for the fatigue crack propagation in FGA, and derived an approximate relation for the fatigue strength or the fatigue life as:

$$(\Delta K_{\text{Inc}})^{m_A} \left(\frac{N_f}{\sqrt{\text{area}_{\text{Inc}}}} \right) = \frac{2}{C_A(m_A - 2)}, \qquad (2)$$

where the subscript "Inc" denotes inclusion.

Hong et al. [25] developed the dislocation model proposed by Tanaka and Mura [32]. By introducing a fraction of an irreversible dislocation, the number of cycles related to crack initiation N_i at inclusion was expressed as:

$$N_i = A \left(\frac{\Delta\sigma - \Delta\sigma_R}{\Delta\sigma} \right)^\alpha \frac{1}{(\Delta\sigma - \Delta\sigma_R)^2 a_{\text{Inc}}}, \qquad (3)$$

where $\Delta\sigma_R$ is the fatigue limit, i.e., the stress range at stress ratio R below which fatigue failure does not occur, $a_{\text{Inc}} = \sqrt{\text{area}_{\text{Inc}}}/2$, A and α are parameters fitted by experimental data.

In this paper, ultrasonic (20 kHz) fatigue tests were performed on specimens of a high-strength steel in a VHCF regime, and a two-parameter model was developed to predict the fatigue life of high-strength steels with fish-eye mode failure in a VHCF regime based on the plastic zone size at the crack tip, for which both the inclusion size and the FGA size at crack origin were considered. An analytical formula was also obtained for predicting the equivalent crack growth rate within the FGA. The predicted results by the model are in good agreement with the data of present experiments and those in the literature. The validity of the predicted results was also discussed.

2 Experimental procedure and results

2.1 Experimental procedure

The experimental material used is a high carbon chromium steel (GCr15). The chemical compositions (mass percentages) are: 1.04 C, 1.51 Cr, 0.29 Mn, 0.24 Si, 0.0058 P, 0.0030 S and the balance is Fe. Specimens were machined into an hourglass shape from the annealed steel bar. The specimens were heated at 845 °C for 1 h in vacuum, and then oil-quenched and tempered for 2 h in vacuum at 180 °C with air cooling.

The tensile test was conducted on five cylindrical specimens with diameters of 6 mm at a strain rate of 10^{-4}s^{-1} by an MTS 810 machine. The average value of the tensile strength is 1896 MPa. The hardness test was performed on three samples by a Vickers hardness tester at a load of 50 g with a load holding time of 15 s. Twenty points were tested for each sample, and the average value was 7.45 GPa.

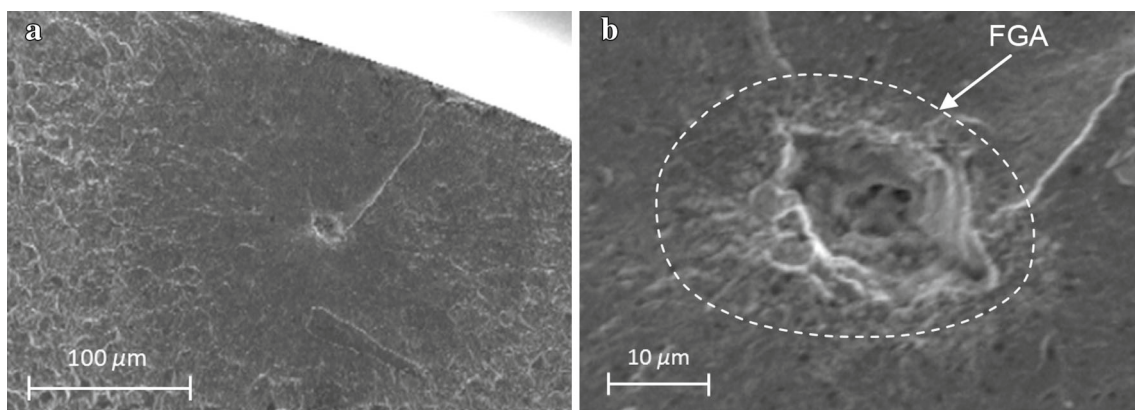Axial fatigue test on hourglass-shape specimens was conducted by using an ultrasonic fatigue test machine at

Fig. 2 Morphology of a broken specimen with FGA surrounding the crack origin in the VHCF regime, $\sigma_a = 989.4$ MPa, $N_f = 1.51 \times 10^8$. **a** Low magnification for the fracture surface with a whole fish-eye. **b** High magnification at crack origin
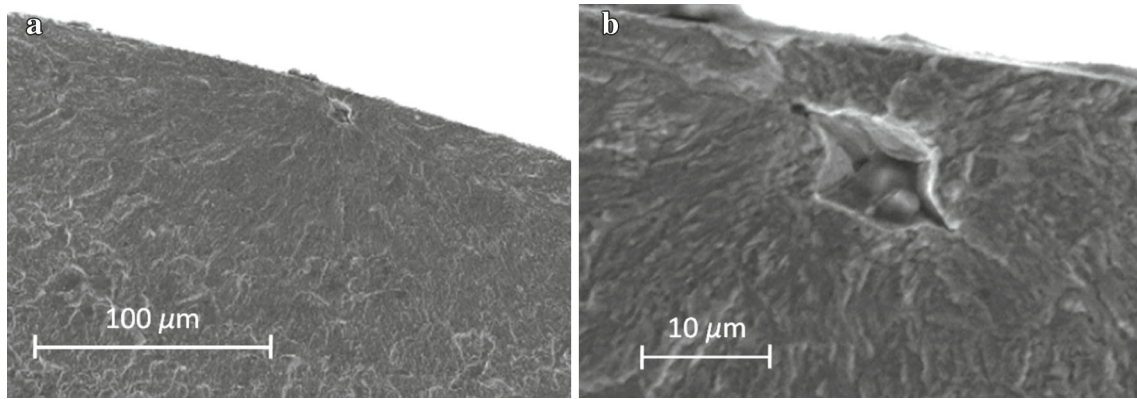
Fig. 3 Morphology of a broken specimen without FGA surrounding a crack origin in the VHCF regime, $\sigma_a = 989.4$ MPa, $N_f = 3.40 \times 10^7$. **a** Low magnification for a fracture surface with a whole fish-eye. **b** High magnification at crack origin
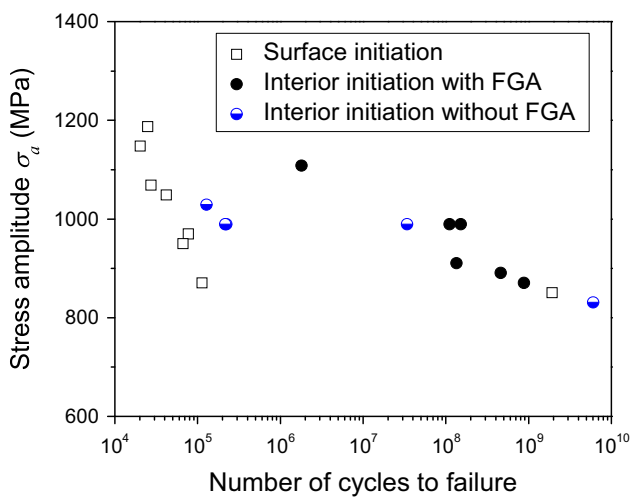

Fig. 4 *S–N* data of tested specimens

a resonance frequency of 20 kHz at room temperature with the stress ratio R of –1. Compressive cold air was used to cool each specimen during the ultrasonic fatigue test. Before a fatigue test, the round notch surface of the specimen was ground and polished to eliminate machine scratches. The geometry of the specimen is shown in Fig. 1.

Fracture surfaces of failed specimens were observed by a field-emission type scanning electron microscope (SEM). The FGA size and the inclusion size at fracture origin were measured from SEM photos by use of Image-Pro Plus software.

2.2 Experimental results

Most of the tested specimens failed from the interior of the specimen with a fish-eye pattern in high-cycle fatigue and VHCF regimes, and the FGA was observed surrounding the fracture origin in most cases. The typical morphology of bro-

ken specimens with and without FGA surrounding the fracture origin in the VHCF regime is presented in Figs. 2 and 3, respectively.

The *S–N* data of the tested specimens are shown in Fig. 4, which indicates that the fatigue life decreases linearly (fatigue life in logarithm scale) with the stress amplitude in the VHCF regime.

3 Model and analysis

Consider a mode-I internal penny crack with diameter d in an infinite solid under a uniform remote tensile stress σ, the maximum size of the plastic zone r_p under the plane strain condition is [33]

$$r_p = \frac{2}{3\pi^2} \left(\frac{\sigma}{\sigma_Y} \right)^2 d, \tag{4}$$

where σ_Y is the yield strength.

In the crack initiation and early growth stage of VHCF, the crack growth rate is much lower than 10^{-10} m/cycle [13,17–20]. This indicates that the crack growth in the FGA region occurs first for the most favorable path and does not always extend in all directions in each fatigue cycle. Here, a fish-eye mode failure with an FGA surrounding the inclusion of the crack origin is considered. The inclusion, FGA, and the crack area after i ($i = 1, 2, \ldots, n$) cycles are approximately treated as internal penny cracks in an infinite solid, and the value of $a_i - a_{i-1}$ ($i = 1, 2, \ldots, n$) is defined as "equivalent crack growth rate", where a_i is the positive square root of the crack area after i cycles, and a_0 is the positive square root of the inclusion projection area perpendicular to the applied stress axis. Further, it is assumed that the equivalent crack growth rate in the FGA region is related to the maximum size of the plastic zone at the crack tip, i.e.,
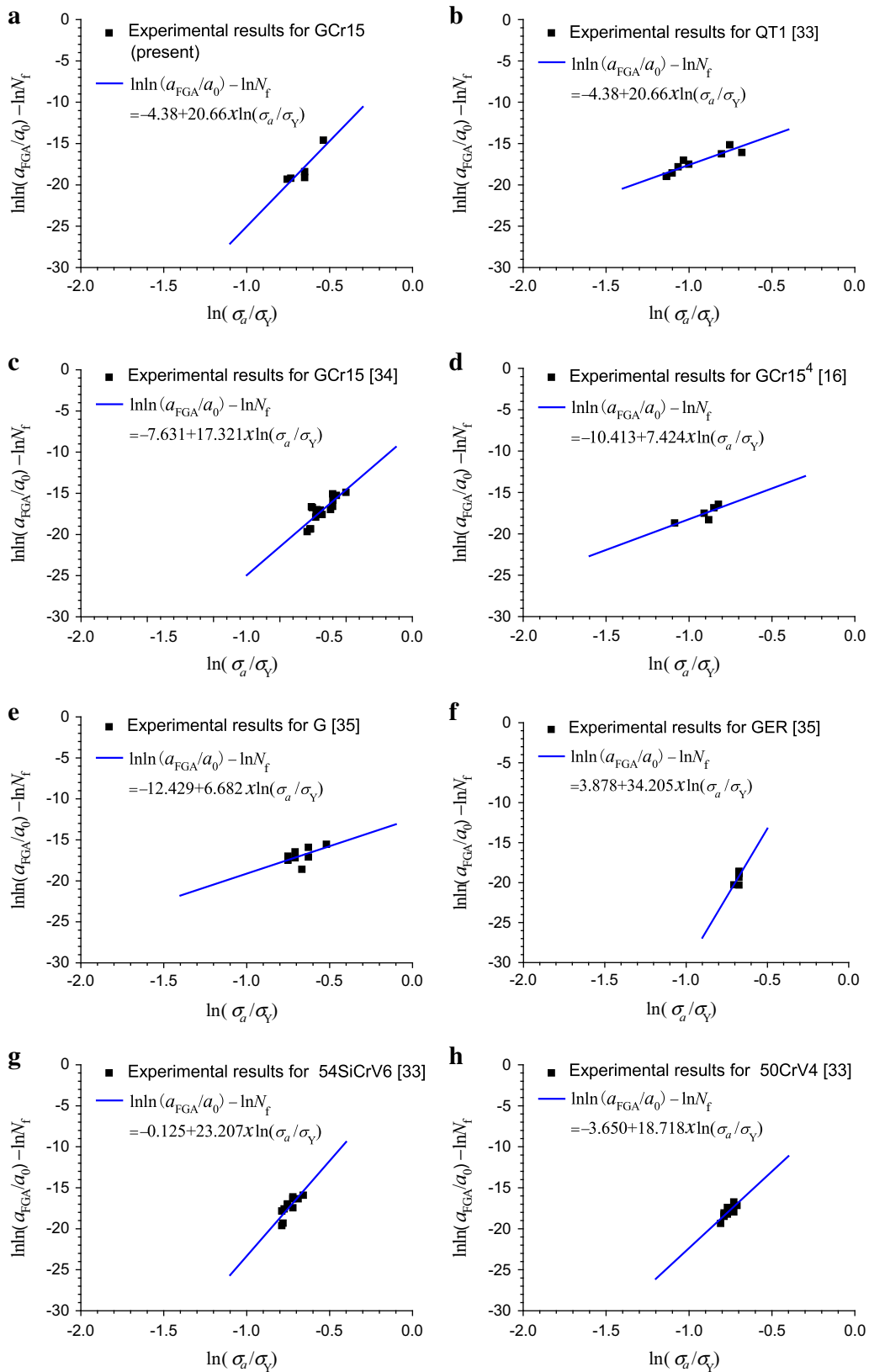
Fig. 5 Experimental values of $N_f^{-1} \ln(a_{FGA}/a_0)$ as a function of σ_a/σ_Y with fitting results in logarithmic scales, in which the superscript 4 denotes the specimens oil-quenched and tempered for 2.5 h in vacuum at 300 °C by the conventional frequency test

$$a_i - a_{i-1} = \frac{2\beta}{3\pi^2} \left(\frac{\sigma_a}{\sigma_Y}\right)^2 \sqrt{\frac{4}{\pi} a_{i-1}^2}$$
$$= \frac{4\beta}{3\pi^{5/2}} \left(\frac{\sigma_a}{\sigma_Y}\right)^2 a_{i-1}, \quad i = 1, 2, \ldots, n, \tag{5}$$

where σ_a is the stress amplitude.

Thus, the equivalent crack length after n cycles is

$$a_n = \left(1 + \frac{4\beta\sigma_a^2}{3\pi^{5/2}\sigma_Y^2}\right)^n a_0. \tag{6}$$

From Eq. (6), the fatigue life N_{FGA} consumed in FGA is obtained by the minimum of the integer n that satisfies

$$\left(1 + \frac{4\beta\sigma_a^2}{3\pi^{5/2}\sigma_Y^2}\right)^n \geq \frac{a_{FGA}}{a_0}, \tag{7}$$

where a_{FGA} is the positive square root of the FGA area.

Equation (7) is solved approximately as

$$N_{FGA} = \frac{1}{\ln(1 + \beta')} \ln \frac{a_{FGA}}{a_0}, \tag{8}$$

where "ln" denotes the natural logarithm, and $\beta' = \frac{4\beta\sigma_a^2}{3\pi^{5/2}\sigma_Y^2}$.

Because of the large value of fatigue life consumed in FGA for high-strength steels in the VHCF regime, the value of β' is much smaller than unity. Taking the Taylor series expansion for $\ln(1 + \beta')$ in Eq. (8), we have

$$N_{FGA} = \frac{1}{\beta'} \ln \frac{a_{FGA}}{a_0} \tag{9}$$

or

$$\beta' = \frac{1}{N_{FGA}} \ln \frac{a_{FGA}}{a_0}. \tag{10}$$

It has been shown that almost all of the fatigue life in the VHCF regime is consumed to form FGA [21–25], so it is reasonable to approximate the fatigue life N_{FGA} consumed in FGA as the total fatigue life N_f.

From the expression of β', it should be at least a function of σ_a/σ_Y, so that $N_f^{-1} \ln(a_{FGA}/a_0)$ is as a function of σ_a/σ_Y. For validating this supposition, Fig. 5 plots the experimental values of $N_f^{-1} \ln(a_{FGA}/a_0)$ as a function of σ_a/σ_Y in logarithmic scales with the fitting results for the present experimental data and the ones available in the literature. For the present material, the value of σ_Y is taken as the value of the tensile strength, which has no effect on the result. It is observed that, for all 8 groups of experimental data, the values of $N_f^{-1} \ln(a_{FGA}/a_0)$ and σ_a/σ_Y are well-approximated by a linear relation in logarithmic scales. This indicates that the stress level is one of the uppermost factors

influencing β' and that β' can be approximated by a power function of σ_a/σ_Y, i.e., $\beta' = \alpha(\sigma_a/\sigma_Y)^l$, where the parameters α and l are determined by fitting the experimental data.

Thus, a two-parameter model for the fatigue life of high-strength steels with fish-eye mode failure in a VHCF regime is derived as

$$N_f = \frac{1}{\alpha} \left(\frac{\sigma_a}{\sigma_Y}\right)^{-l} \ln \frac{a_{FGA}}{a_0}. \tag{11}$$

It is seen from Eq. (11) that the fatigue life is dependent on the relative size of FGA to inclusion, and increases with increasing the relative size of FGA to inclusion [15].

Further, an approximate analytical formula is derived from Eq. (6) for the equivalent crack growth rate in FGA

$$\frac{da}{dN} = \alpha \left(\frac{\sigma_a}{\sigma_Y}\right)^l a. \tag{12}$$

Equation (12) indicates that the equivalent crack growth rate in FGA could be described via a simple log-linear relationship, i.e.,

$$\ln a = \lambda N + \ln a_0, \tag{13}$$

where $\lambda = \alpha(\sigma_a/\sigma_Y)^l$.

Equation (13) has the same form as the Frost and Dugdale relation [36], which has been successfully used to predict the growth of near micrometer-sized cracks for steels and aluminium alloys [37]. This indicates that the equivalent crack growth rate in FGA accords with the Frost and Dugdale relation.

4 Model results and discussion

4.1 FGA size estimation

It is noted from Eq. (11) that the inclusion size and the FGA size are the premise for the prediction. For inclusion size, it can be estimated by experimental observation and statistical method [38,39]. Regarding the estimation of FGA size, our recent investigations [16,25] and other attempts [14,22,40] have shown that the stress intensity factor range at the front of FGA ΔK_{FGA} remains almost a constant and corresponds to the threshold value of the crack propagation ΔK_{th}, in which ΔK_{FGA} is calculated by $\Delta K_{FGA} = 0.5\sigma_a\sqrt{\pi \sqrt{area_{FGA}}}$.

Figure 6 plots the ratio of experimental value ΔK_{FGA} to the mean value of $\Delta K'_{FGA}$ (in MPa·m$^{1/2}$) versus fatigue life for the present experimental data along with those from the literature. For all the 17 groups of experimental data shown in Fig. 6, the experimental value is close to its mean value
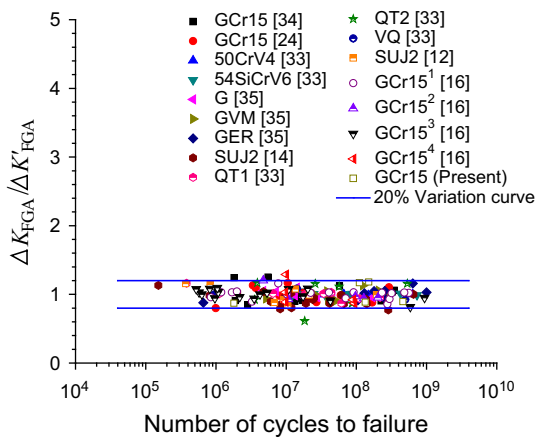
Fig. 6 Ratio of experimental value ΔK_{FGA} to mean value $\Delta K'_{FGA}$ versus fatigue life for present experimental data and those from the literature, in which the superscripts 1 and 2 denote the specimens by oil-quenching and tempering for 2.5 h in a vacuum at 150 °C under an ultrasonic test and a conventional frequency test, respectively, and the superscripts 3 and 4 denote the specimens by oil-quenching and tempering for 2.5 h in a vacuum at 300 °C under an ultrasonic test and a conventional frequency test, respectively
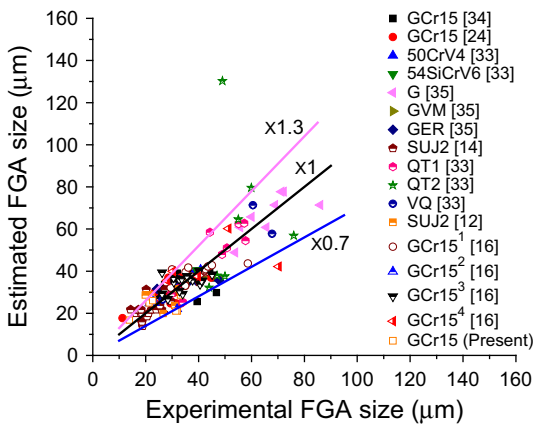

Fig. 7 Estimated FGA sizes as a function of the experimental data for each group of experimental results in Fig. 6, in which the superscripts 1 and 2 denote the specimens by oil-quenching and tempering for 2.5 h in a vacuum at 150 °C under an ultrasonic test and a conventional frequency test, respectively, and the superscripts 3 and 4 denote the specimens by oil-quenching and tempering for 2.5 h in a vacuum at 300 °C under an ultrasonic test and a conventional frequency test, respectively

$\Delta K'_{FGA}$, the relative difference is within 20 % except for a few experimental points. This result further indicates that the stress intensity factor range at the front of the FGA reflects the propensity of the materials, which can be regarded as a constant independent of the stress amplitude and the fatigue life. It also shows that, for high-strength steels with fish-eye mode failure, the FGA size could be obtained by the stress intensity factor range at the front of the FGA and the stress amplitude. For clarity, Fig. 7 plots the estimated FGA size as a function of the experimental value associated with Fig. 6, in which the estimated FGA size is obtained by $\Delta K'_{FGA} =$
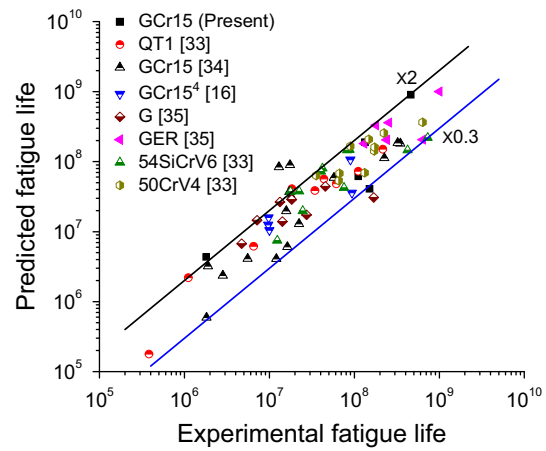

Fig. 8 Comparison of predicted fatigue life by the proposed model using the experimental FGA size and the inclusion size with eight groups of experimental data in Fig. 5, in which the superscript 4 denotes the specimens by oil-quenching and tempering for 2.5 h in a vacuum at 300 °C by a conventional frequency test

$0.5\sigma_a\sqrt{\pi\sqrt{area_{FGA}}}$. It is seen that the estimated FGA sizes are in good agreement with the experimental ones for all the 17 groups of experimental results, the relative errors of which are almost within 30 %. Therefore, the FGA size can be obtained through the stress intensity factor range at the front of the FGA and the stress amplitude for VHCF of high-strength steels with fish-eye mode failure.

It is noted that the results by Paris et al. [41] and Marines-Garcia et al. [42] showed that at the threshold corner location:

$$\frac{da}{dN} = b \text{ and } \frac{\Delta K_{eff}}{E\sqrt{b}} = 1, \tag{14}$$

where b is the magnitude of Burger's vector and E is the elastic modulus.

From Eq. (14), the threshold value is obtained as

$$\Delta K_{eff,th} = E\sqrt{b}. \tag{15}$$

For high-strength steels, taking $E = 208$ MPa, we have $\Delta K_{eff,th} \approx 3.3$ MPa $\cdot$ m$^{1/2}$. The mean value of $\Delta K'_{FGA}$ for the 17 groups of experimental data shown in Fig. 6 is in the range of 3.54–5.69. This indicates that the threshold value of $\Delta K_{eff,th} \approx 3.3$ MPa $\cdot$ m$^{1/2}$ obtained by Paris et al. [41] and Marines-Garcia et al. [42] may be regarded as the lower bounder of the stress intensity factor range at the front of the FGA.

4.2 Fatigue life estimation

Figure 8 shows the comparison of predicted fatigue life by the present model using the experimental FGA size and the inclusion size with the eight groups of experimental data in
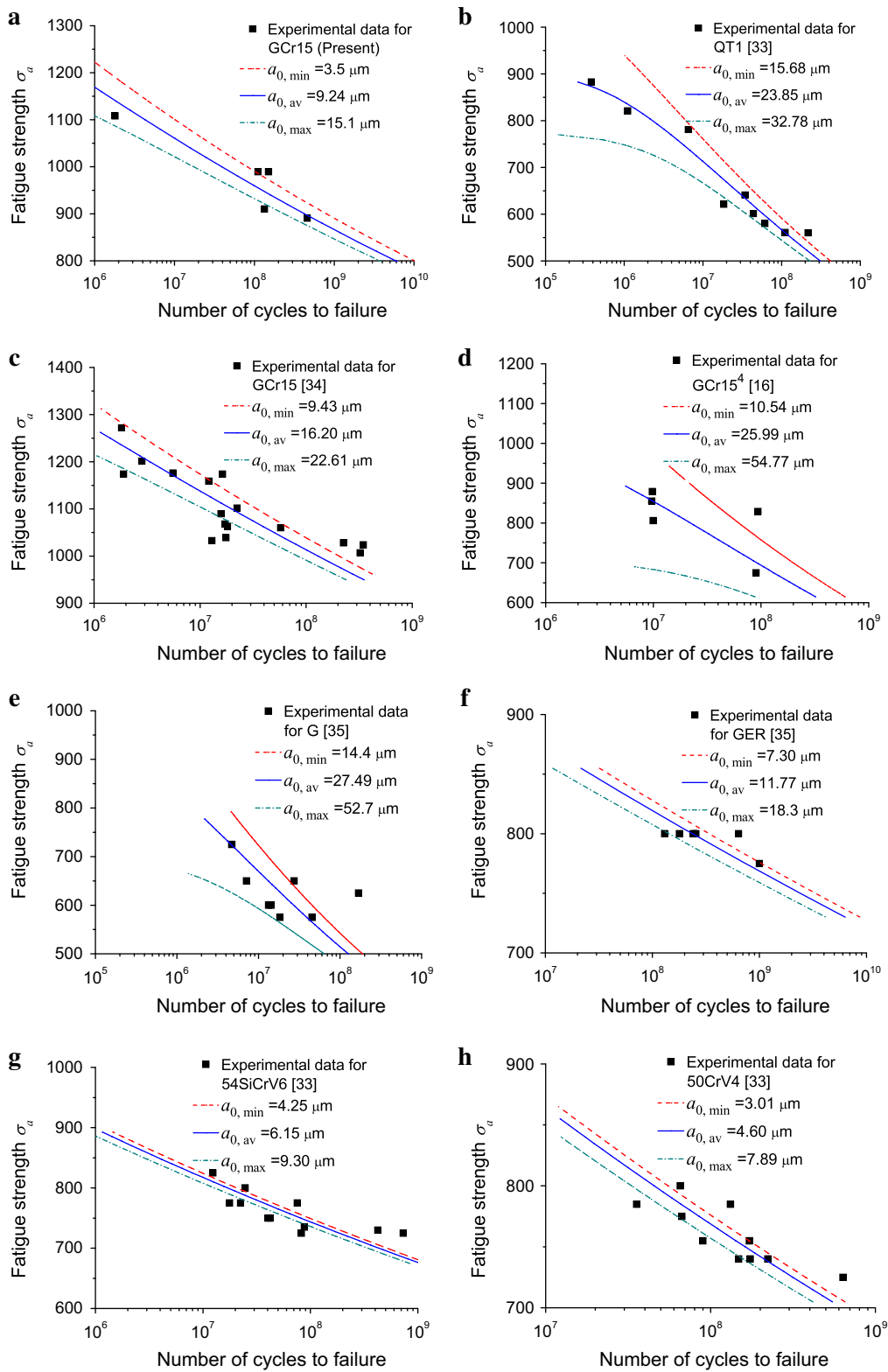
Fig. 9 Comparison of predicted fatigue life by the present model using the estimated FGA size and different inclusion size with the eight groups of experimental data in Fig. 5, in which $a_{0,\min}$ is the minimum, $a_{0,\mathrm{av}}$ is the average, $a_{0,\max}$ is the maximum of the inclusion sizes at the crack origin, and the superscript 4 denotes the specimens by oil-quenching and tempereing for 2.5 h in a vacuum at 300 °C by a conventional frequency test

Fig. 5. It is seen that the predicted fatigue life is in agreement with the experimental one, indicating that the proposed two-parameter model is capable of correlating the fatigue life, the fatigue strength and the microstructure parameters (inclusion size and FGA size) at the fracture origin.

Figure 9 shows a further comparison of predicted fatigue life by the present model using the estimated FGA size and different inclusion sizes with the experimental ones in Fig. 5. It is seen from Fig. 9 that the present model reflects the effect of inclusion size on fatigue life, and the predicted fatigue life is in good agreement with the experimental data. The predicted fatigue life with the minimum inclusion size is generally higher than the experimental value, while the predicted fatigue life with the maximum inclusion size is generally smaller than the experimental value. For the materials in (Fig. 9a, b, d–f), the predicted fatigue life by the present model with the maximum inclusion size seems to be conservative. Figure 9 also shows that the predicted S–N curve with the average inclusion size is moderate and close to the median S–N curve.

It is noted that the shape of the S–N curve for high-strength steels often presents a duplex pattern corresponding to a surface-initiated fracture mode and an interior-initiated fracture mode [14,24,40]. In this paper, only the interior-initiated fracture mode with an FGA surrounding the inclusion at the crack origin is considered. Hence, the present model is not applicable for the prediction of the fatigue life for the samples with the activated inclusion size bigger than the FGA size, for which the FGA is impossible to form around the inclusion.

4.3 Analysis of the predicted results

Normally, the inclusion size and the FGA size used in the model are not the same values as the ones at the crack origin, namely, that the inclusion size and the FGA size used in the model often have some deviation from those at the real crack region occurring in the cycling process. In the following, the effect of the variation of inclusion size and FGA size with the predicted results is discussed. Equation (11) suggests that the validity of the predicted results is indicated by the effect of the variation of inclusion size and FGA size with the value of $\ln(a_{FGA}/a_0)$. Figure 10 plots the value of $\ln(a_{FGA}/a_0)$ as a function of a_{FGA}/a_0. It is seen from Fig. 10 that, for the FGA size several times larger than the inclusion size, the variation of the inclusion size or the FGA size has a small influence on the predicted fatigue life. For such a case, the present model gives good predicted results. While for the FGA size close to the inclusion size, the variation of the inclusion size or the FGA size has a substantial influence on the predicted results.
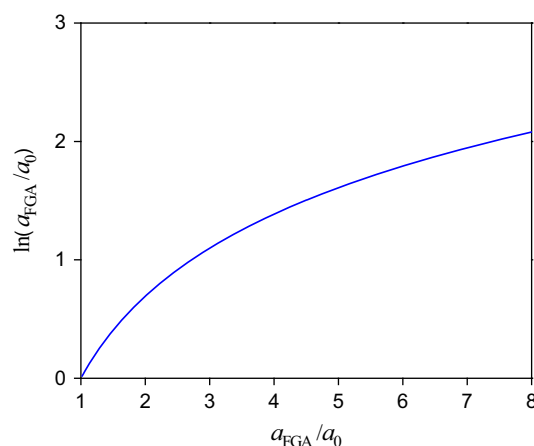

Fig. 10 Value of $\ln(a_{FGA}/a_0)$ as a function of a_{FGA}/a_0

5 Conclusions

In this paper, a two-parameter model involving two microscopic parameters (inclusion size and FGA size) at the crack origin is proposed for predicting the fatigue life of high-strength steels with fish-eye mode failure in a VHCF regime based on plastic zone size at the crack tip. The model reflects the effect of inclusion size on fatigue life, and the predicted results are in good agreement with experimental data. The paper indicates that the effect of inclusion size on the fatigue life is related to the relative size of FGA to the inclusion.

Moreover, through the comparison of the experimental values of ΔK_{FGA} with the average experimental value of $\Delta K'_{FGA}$, it is shown that the stress intensity factor range at the front of the FGA is a constant, which is irrespective of the stress amplitude and fatigue life, and that the FGA size can be obtained by the stress intensity factor range at the front of the FGA and the stress amplitude for high-strength steels with fish-eye mode failure in a VHCF regime.

References

1. Bathias, C., Drouillac, L., Le Francois, P.: How and why the fatigue S-N curve does not approach a horizontal asymptote. Int. J. Fatigue **23**, S143–151 (2001)
2. Hong, Y., Zhao, A., Qian, G.: Essential characteristic and influential factors for very-high-cycle fatigue behavior of metallic materials. Acta Metall. Sin. **45**, 769–780 (2009)
3. Duan, Z., Ma, X.F., Shi, H.J., et al.: Gigacycle fatigue behaviors of two SNCM439 steels with different tensile strengths. Acta Mech. Sin. **27**, 778–784 (2011)
4. Huang, Z.Y., Wang, Q.Y., Wagner, D., et al.: A rapid scatter prediction method for very high cycle fatigue. Fatigue Fract. Eng. Mater. Struct. **36**, 462–468 (2013)

5. Murakami, Y., Matsunaga, H., Abyazi, A., et al.: Defect size dependence on threshold stress intensity for high-strength steel with internal hydrogen. Fatigue Fract. Eng. Mater. Struct. **36**, 836–850 (2013)

6. Lei, Z., Xie, J., Sun, C., et al.: Effect of loading condition on very-high-cycle fatigue behavior and dominant variable analysis. Sci. China-Phys. Mech. Astron. **57**, 74–82 (2014)

7. Sun, C., Lei, Z., Hong, Y.: Effects of stress ratio on crack growth rate and fatigue strength for high cycle and very-high-cycle fatigue of metallic materials. Mech. Mater. **69**, 227–236 (2014)

8. Li, S.X., Zhang, P.Y., Yu, S.R.: Experimental study on very high cycle fatigue of martensitic steel of 2Cr13 under corrosive environment. Fatigue Fract. Eng. Mater. Struct. **37**, 1146–1152 (2014)

9. Shanyavskiy, A.A.: Very-high-cycle-fatigue of in-service air-engine blades, compressor and turbine. Sci. China-Phys. Mech. Astron. **57**, 19–29 (2014)

10. Shyam, A., Blau, P., Jordan, T., et al.: Effect of submillimeter size holes on the fatigue limit of a high strength tool steel. Fatigue Fract. Eng. Mater. Struct. **37**, 368–379 (2014)

11. Liu, X., Sun, C., Hong, Y.: Effects of stress ratio on high cycle and very-high-cycle fatigue behavior of a Ti-6Al-4V alloy. Mater. Sci. Eng. **622**, 228–235 (2015)

12. Sakai, T., Sato, Y., Oguma, N., et al.: Characteristic S–N properties of high-carbon-chromium-bearing steel under axial loading in long-life fatigue. Fatigue Fract. Eng. Mater. Struct. **25**, 765–773 (2002)

13. Murakami, Y., Nomoto, T., Ueda, T.: Factors influencing the mechanism of superlong fatigue failure in steels. Fatigue Fract. Eng. Mater. Struct. **22**, 581–590 (1999)

14. Shiozawa, K., Lu, L., Ishihara, S., et al.: S–N curve characteristics and subsurface crack initiation behaviour in ultra-long life fatigue of a high carbon-chromium bearing steel. Fatigue Fract. Eng. Mater. Struct. **24**, 781–790 (2001)

15. Murakami, Y., Nomoto, T., Ueda, T.: On the mechanism of fatigue failure in the superlong life regime (N 10^7 cycles). Part I: influence of hydrogen trapped by inclusions. Fatigue Fract. Eng. Mater. Struct. **23**, 893–902 (2000)

16. Zhao, A., Xie, J., Sun, C., et al.: Prediction of threshold value for FGA formation. Mater. Sci. Eng. A **528**, 6872–6877 (2011)

17. Tanaka, K., Akiniwa, Y.: Fatigue crack propagation behaviour derived from S–N data in very high cycle regime. Fatigue Fract. Eng. Mater. Struct. **25**, 775–784 (2002)

18. Pippan, R., Tabernig, B., Gach, E., et al.: Non-propagation conditions for fatigue cracks and fatigue in the very high-cycle regime. Fatigue Fract. Eng. Mater. Struct. **25**, 805–811 (2002)

19. Ogawa, T., Stanzl-Tschegg, S.E., Schönbauer, B.M., et al.: A fracture mechanics approach to interior fatigue crack growth in the very high cycle regime. Eng. Fract. Mech. **115**, 241–254 (2014)

20. Sander, M., Müller, T., Lebahn, J., et al.: Influence of mean stress and variable amplitude loading on the fatigue behaviour of a high-strength steel in VHCF regime. Int. J. Fatigue **62**, 10–20 (2014)

21. Chapetti, M.D., Tagawa, T., Miyata, T.: Ultra-long cycle fatigue of high-strength carbon steels part I: review and analysis of the mechanism of failure. Mater. Sci. Eng. A **356**, 227–235 (2003)

22. Shiozawa, K., Morii, Y., Nishino, S., et al.: Subsurface crack initiation and propagation mechanism in high strength steel in a very high cycle fatigue regime. Int. J. Fatigue **28**, 1521–1532 (2006)

23. Wagner, D., Ranc, N., Bathias, C., et al.: Fatigue crack initiation detection by an infrared thermography method. Fatigue Fract. Eng. Mater. Struct. **33**, 12–21 (2009)

24. Li, W., Sakai, T., Li, Q., et al.: Reliability evaluation on very high cycle fatigue property of GCr15 bearing steel. Int. J. Fatigue **32**, 1096–1107 (2010)

25. Hong, Y., Lei, Z., Sun, C., et al.: Propensities of crack interior initiation and early growth for very-high-cycle fatigue of high strength steels. Int. J. Fatigue **58**, 144–151 (2014)

26. Liu, Y.B., Li, Y.D., Li, S.X., et al.: Prediction of the S–N curves of high-strength steels in the very high cycle fatigue regime. Int. J. Fatigue **32**, 1351–1357 (2010)

27. Sun, C., Xie, J., Zhao, A., et al.: A cumulative damage model for fatigue life estimation of high-strength steels in high-cycle and very-high-cycle fatigue regimes. Fatigue Fract. Eng. Mater. Struct. **35**, 638–647 (2012)

28. Sun, C., Lei, Z., Xie, J., et al.: Effects of inclusion size and stress ratio on fatigue strength for high-strength steels with fish-eye mode failure. Int. J. Fatigue **48**, 19–27 (2013)

29. Wang, Q.Y., Bathias, C., Kawagoishi, N., et al.: Effect of inclusion on subsurface crack initiation and gigacycle fatigue strength. Int. J. Fatigue **24**, 1269–1274 (2002)

30. Murakami, Y., Endo, M.: Effects of defects, inclusions and inhomogeneities on fatigue strength. Int. J. Fatigue **16**, 163–182 (1994)

31. Akiniwa, Y., Miyamoto, N., Tsuru, H., et al.: Notch effect on fatigue strength reduction of bearing steel in the very high cycle regime. Int. J. Fatigue **28**, 1555–1565 (2006)

32. Tanaka, K., Mura, T.: A theory of fatigue crack initiation at inclusions. Metall. Trans. A **13A**, 117–123 (1982)

33. Yang, Z.G., Li, S.X., Liu, Y.B., et al.: Estimation of the size of GBF area on fracture surface for high strength steels in very high cycle fatigue regime. Int. J. Fatigue **30**, 1016–1023 (2008)

34. Hong, Y.S., Zhao, A.G., Qian, G.A., et al.: Fatigue strength and crack initiation mechanism of very-high-cycle fatigue for low alloy steels. Metall. Mater. Trans. A **43**, 2753–2762 (2012)

35. Li, Y.D., Yang, Z.G., Li, S.X., et al.: Correlations between very high cycle fatigue properties and inclusions of GCr15 bearing Steel. Acta Metall. Sin. **44**, 968–972 (2008)

36. Frost, N.E., Dugdale, D.S.: The propagation of fatigue cracks in sheet specimens. J. Mech. Phys. Solids **6**, 92–110 (1958)

37. Jones, R., Molent, L., Pitt, S.: Similitude and the Paris crack growth law. Int. J. Fatigue **30**, 1873–1880 (2008)

38. Atkinson, H.V., Shi, G.: Characterization of inclusions in clean steels: a review including the statistics of extremes methods. Prog. Mater. Sci. **48**, 457–520 (2003)

39. Nakajima, M., Tokaji, K., Itoga, H., et al.: Effect of loading condition on very high cycle fatigue behavior in a high strength steel. Int. J. Fatigue **32**, 475–480 (2010)

40. Sakai, T.: Review and prospects for current studies on very high cycle fatigue of metallic materials for machine structural use. J. Solid Mech. Mater. Eng. **3**, 425–439 (2009)

41. Paris, P.C., Marines-Garcia, I., Hertzberg, R.W., et al.: The relationship of effective stress intensity, elastic modulus and Burgers-vector on fatigue crack growth as associated with "fish eye" gigacycle fatigue phenomena. In: Proceedings of the international conference on very high cycle fatigue III, Kyoto (2004)

42. Marines-Garcia, I., Paris, P.C., Tada, H., et al.: Fatigue crack growth from small to large cracks on very high cycle fatigue with fish-eye failures. Eng. Fract. Mech. **75**, 1657–1665 (2008)